Journal of Molecular Structure 1338 (2025) 142270

Contents lists available at ScienceDirect

Journal of Molecular Structure

journal homepage: www.elsevier.com/locate/molstr

Systematically study of ligands field effect on a pseudo-D_{6h} Dy(III) single-ion magnet with axially asymmetric ligands

Xiang Zhong [a,1], Rajanikanta Rana [b,1], Tong-Kai Luo [a], Yan- Fang Wu [a], Yan Peng [a,*], Sui-Jun Liu [a,*], Gopalan Rajaraman [b,*], He-Rui Wen [a]

[a] School of Chemistry and Chemical Engineering, Jiangxi Provincial Key Laboratory of Functional Crystalline Materials Chemistry, Jiangxi University of Science and Technology, Ganzhou 341000, Jiangxi Province, PR China

[b] Department of Chemistry, Indian Institute of Technology Bombay, Powai, Mumbai 400076, Mumbai, India

ARTICLE INFO

Keywords:
Pseudo-D_{6h}
Single-ion magnet
Schiff base circular
Ab initio calculations

ABSTRACT

A pseudo-D_{6h} Dy(III) single-ion magnet (SIM) with axially asymmetric ligands was synthesized based on Schiff base cyclic (L^{N6}) ligand, which is rare seen in D_{6h} single-ion magnets system. This complex shows field-induced SMM behavior with U_{eff} of 36.58 K and τ_0 of 1.91×10^{-5} s. *Ab initio* calculations indicate the poor SMM behavior is due to quantum tunnelling of magnetization triggered by the mixture of the ground state $m_J = \pm 15/2$ and $m_J = \pm 7/2$ state. Based on this complex, *ab initio* calculations were performed to systematically investigate the effect of ligands on the magnetic properties, offering new design criteria to enhance D_{6h} SIM performance.

1. Introduction

Single-molecule magnets (SMMs) have attracted widespread attention because of their potential applications in high-density information storage [1–2], quantum computing [3–4], molecular spintronics [5–6]. Due to the unique 4*f* electronic properties of lanthanide, most of the lanthanide ions have strong spin-orbit coupling and large ground state, which are considered ideal candidates for the construction of SMMs [7–14]. Thus, there is continuous interest in assembling Ln-SMMs, especially for lanthanide single-ion magnets (Ln-SIMs). There has been very promising progress in recent years, with magnetic hysteresis observed up to 80 K [15–16]. As is well known, in addition to the choice of central metal ions, the design of the coordination environment for the central metal ion is also crucial for the performance of Ln-SMMs, especially for Ln-SIMs. According to theoretical calculations, lanthanide mononuclear complexes with ligand field showing axial point group symmetry, such as trigonal prisms (D_{3h}) [17–18], square antiprism (D_{4d}) [19–21], octahedrons (D_{4h}) [22–24], pentagonal bipyramidal (D_{5h}) [25–33], hexagonal bipyramidal (D_{6h}) [34–43] and so on [44–45] are considered to be an effective way to slow down magnetization relaxation by reducing transverse magnetic anisotropy. However, among the large number of complexes with axial point group symmetry, there are only a few cases with axially asymmetric ligands. For example, in 2018, Zheng et al. reported a D_{5h} Dy(III) SIM complex $[Dy(^tBuO)Cl(THF)_5][BPh_4]\cdot 2THF$, in which the equatorial plane was formed by five THF molecules, and the axial directions were occupied by Cl^- and $^tBuO^-$ [30]. In 2022, Chen et al. reported a D_{6h} Dy(III) SIM with axially asymmetric ligands of Ph_3SiO^- and Cl^-, which shows great potential for Ln-SIMs [46]. However, the effects of axially asymmetric ligand field on magnetic properties of such complexes have not been studied in detail.

Herein, we report an axially asymmetric lanthanide mononuclear complex $[DyL^{N6}(Ph_3SiO)(CH_3COO)](PF_6)\cdot 3H_2O$ (**1**) based on Schiff base cyclic (L^{N6}) ligand (Fig. 1). It is a nine-coordinate complex with a coordination configuration close to the spherical relaxed capped cube (Fig. S2 in Supporting information). Magnetic measurements indicate that complex **1** is not a SIM under zero dc field. However, it is a field-induced SIM with effective energy barrier (U_{eff}) of 36.58 K. Moreover, *ab* initio calculations were performed to explain the magnetic behavior for complex **1**. Furthermore, based on this complex, *ab* initio calculations were performed to systematically investigate the ligand field effect on the magnetic properties of this system.

Complex **1** crystallizes in the monoclinic $P2_1/m$ space group (Table S1 in Supporting information) and the asymmetric unit contains two independent molecules (Fig. S3 in Supporting information). The Dy•••Dy distance between the two molecules is 8.5264(4) Å. Each Dy^{III} is nine-coordinate Hula-hoop (HH) coordination geometry with

* Corresponding authors.
E-mail addresses: py16882020@163.com (Y. Peng), sjliu@jxust.edu.cn (S.-J. Liu), rajaraman@chem.iitb.ac.in (G. Rajaraman).
[1] These authors contributed equally to this work and should be considered co-first authors.

https://doi.org/10.1016/j.molstruc.2025.142270
Received 18 January 2025; Received in revised form 24 February 2025; Accepted 1 April 2025
Available online 2 April 2025

deviation value of 2.008 (Table S2 in Supporting information) according to the Shape analysis. As shown in Fig. 1, the hexagonal heterocyclic ligand is as a distorted equatorial plane, the axial directions are occupied by Ph_3SiO^- and CH_3COO^- (OAc^-), respectively. In the equatorial plane of the L^{N6} ligand, the Dy-N distances range from 2.5585(8) to 2.6034(6) Å. In the axial directions, Dy^{III} ion coordinated with Ph_3SiO^- to form a shorter Dy-O bond with a bond length of 2.1024(7) Å, while Dy^{III} ion coordinated with CH_3COO^- to form a longer bond with a bond length of 2.4022(7) Å (Table S3 in Supporting information).

The dc susceptibilities of complex **1** were measured in temperature range 2–300 K under 500 Oe dc field. At 300 K, the $\chi_M T$ value is 14.14 cm^3 K mol^{-1}, which is in good agreement with the expected value of 14.17 cm^3 K mol^{-1} for one free Dy^{III} ion. Upon cooling, the $\chi_M T$ value keeps almost constant from 300 to 110 K and decreases rapidly after 110 K, reaching a minimum value of 11.40 cm^3 K mol^{-1} at 2 K (Fig. S4 in Supporting information). In the meantime, the isothermal field-dependent magnetization (M/H) was measured at 2, 3 and 5 K in the field range of 0–7 T. The value of magnetization at 2 K and 7 T was determined, and the result shows that the maximum magnetization can reach 5.4 μ_B, significantly lower than the theoretical value of 10 μ_B for one free Dy^{III} ion ($g_J \times J = 15/2 \times 4/3 = 10\ \mu_B$), suggesting the presence of magnetic anisotropy within the complex.

AC magnetic susceptibilities were measured for complex **1** in order to investigate the SIM properties (Fig 2 and Fig S6-S8 in Supporting information). Under zero dc field, the complex does not exhibit single-molecule magnetic properties probably due to the severe QTM (Fig. S6 in Supporting information). Therefore, dc fields were applied to measure the ac susceptibilities, and a dc field of 500 Oe was determined as the optimal field. In the optimal field, both in-phase (χ_M') and out-of-phase (χ_M'') show peaks (Fig. 2). Thus, the magnetic relaxation time, τ, can be fitted from Cole-Cole plots using generalized Debye model (Fig. S7 in Supporting information), which gave α values in the range of 0.040–0.72 (2–16 K) (Table S4 in Supporting information). The τ^{-1} vs T plot was fitting with equation of $\tau^{-1} = \tau_{QTM}^{-1} + CT^n + \tau_0^{-1}\exp(-U_{eff}/T)$, in which C and n are Raman process parameters and τ_{QTM} is QTM rate. The best fit gave parameters of $U_{eff} = 36.58$ K, $\tau_0 = 1.91 \times 10^{-5}$ s, $C = 0.00116\ s^{-1}\ K^{-n}$, $n = 5.33$, $\tau_{QTM} = 0.1$ s (Fig. S8 in Supporting information).

Fig. 3

To elucidate the relaxation mechanism and electronic structure of complex **1**, the MOLCAS 8.2 software was employed to carry out *ab initio* CASSCF/RASSI-SO/SINGLE_ANISO calculations (computational details in Supporting information). The calculations reveal that the complex ground Kramers doublet (KD) is Ising in nature ($g_{zz} = 19.96$, $g_6 = 0.01$, $g_{xx} = 0.01$), and this is in line with earlier D_{6h} molecule published [34, 47]. The composition of the ground state is predominantly $m_J = \pm 15/2$,

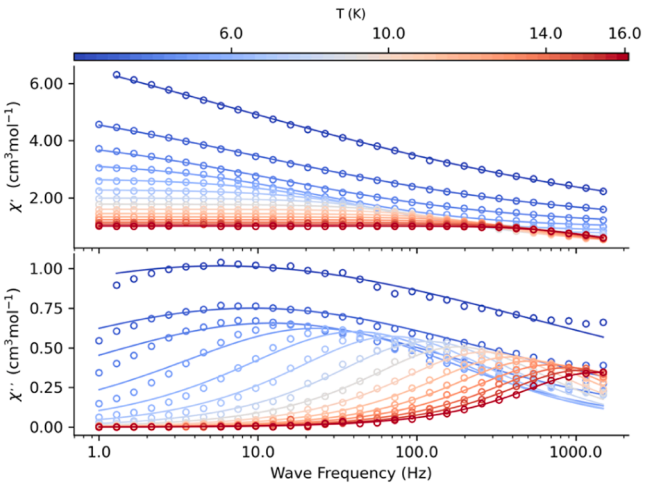

Fig. 2. Variable frequency in-phase (upper) and out-of-phase (lower) magnetic susceptibility of **1**, in the static field of 500 Oe and an oscillating field of 3 Oe.

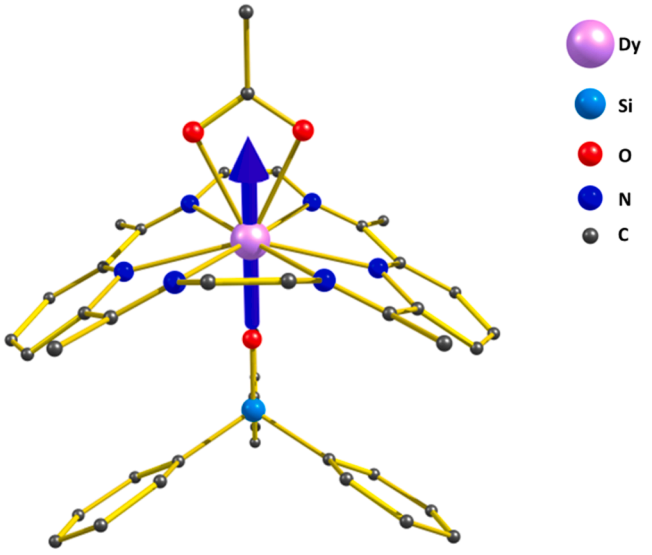

Fig. 3. Orientation of the magnetic anisotropy axis (g_{zz}) of **1**. Hydrogen atoms and solvent molecules are omitted for clarity.

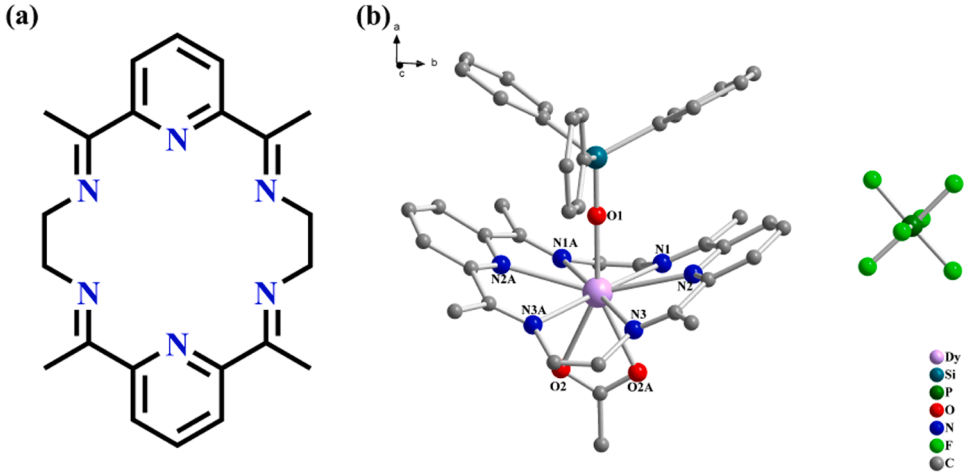

Fig. 1. (a) The macrocyclic ligand L^{N6}; (b) molecular structure of **1** with one Ph_3SiO^- axial ligand and one CH_3COO^- axial ligand and the polydentate ligand L^{N6} in the equatorial plane. Hydrogen atoms and solvent molecules are omitted for clarity.

which is mixing with the $m_J = \pm 7/2$ state (see Table S5-S18 in Supporting information). Although the transverse anisotropy is relatively smaller, this is sufficient to trigger quantum tunnelling of magnetization as revealed by the computed QTM probability of the ground state KD, Supporting the absence of out of phase signal in the absence of applied magnetic field. However, as the QTM probability is smaller, a relatively small magnetic field can quench the tunnelling, as observed in the experiments. However, the expected barrier height is relatively smaller. Furthermore, the first excited KD g-tensors were found to have a significant transverse component ($g_{zz} = 16.67$, $g_{yy} = 0.38$, $g_{xx} = 0.63$), that diminish the prospect of **1** being a good SIM also relaxation occurs predominantly in the 2nd KDs (Fig 4). Furthermore, the estimated the crystal field parameters using the Hamiltonian $\widehat{H}_{CF} = \sum_{k=2,4,6} \sum_{q=-k}^{q=k} B_k^q \widehat{O}_k^q$ (here B_k^q is the crystal field parameter and $\widehat{O}_k^q$ is the Stevens operator respectively) for **1** suggest comparable axial crystal field (CF) parameter ($k = 2, 4, 6$; $q = 0$) with non-axial ($k = 2, 4, 6$; $q \neq 0$), reflecting a weak SIM behaviour (Table S19 in Supporting information). This is due to the non-planarity of the equatorial ligand and relatively weaker axial ligands. For comparison, the previously reported related D_{6h} complex relax via the second excited state with a much larger ground state to first excited state gap (620 cm^{-1} vs 392 cm^{-1}) [47].

As **1** does not exhibit good SIM characteristics, we decided to perform in silico modelling of the axial ligand to predict a suitable ligand that can yield superior SIM characteristics. In this model, we have substituted the OAc^- ligand with a linear ligand, such as the $OSiPh_3$, which can offer strong axiality and yield a favourable geometry. Further modelling was performed, replacing the axial group by acac (model **1a**), nitrate (model **1b**), -Cl (model **1c**), F (model **1d**), -OH (model **1e**), OPh_^{t}Bu$_2$ (model **1f**), OPh_^{t}Bu$_3$ (model **1 g**), OSi^{t}Bu (model **1h**), OC^{t}Bu (model **1i**), $OCPh_3$ (model **1j**), $OSiPh_3$ (model **1k**), H_2O (model **1l**). These geometries were optimized using the DFT method (B3LYP/6–31G*; see computational details).

The substitution of OAc^- ligands with F **1d** and OH **1e** ligands, characterized by their strong ligand properties, has a profound impact. The considerable increase in the barrier height is a direct result of the strong axial and weak equatorial bonds, which are influenced by the oblate shape of Dy's electron density. Moreover, small and strong axial ligands induce planarity in the equatorial bonds, enhancing the system's anisotropy. This is evident in the considerably higher axial crystal field parameter than the non-axial crystal field parameter. (Table S24–25 in Supporting information). In the case of complex **1d** and **1e**, the 1st, 2nd, and 3rd Kramer's doublets (KDs) consist of m_J values $\pm 15/2$, $\pm 13/2$, and $\pm 11/2$. However, starting from the 4th KD onwards, a mixing of states becomes evident, as indicated in Table S10–11. Therefore, relaxation occurs predominantly in the 4th KDs for both ligands. This observation is further supported by the relaxation mechanism illustrated in Fig S10 (f-g) for models **1d** and **1e**, respectively. To clarify further, we generated a plot (Fig S9(a-n) in Supporting information) illustrating the anisotropy axis for all optimized geometries. Notably, when the ligands were either OH or F, it was observed that the anisotropy axis aligned with the Dy-F or Dy-OH bond. This alignment suggests that the presence of OH and F ligands enhances the anisotropy of the complex.

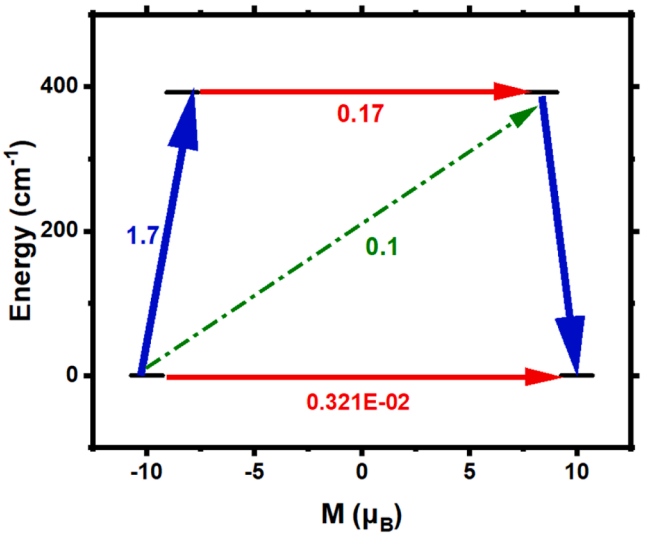

Fig. 4. Magnetic relaxation in **1** involves multiple pathways: Kramer's doublet (KD), QTM/TA-QTM via ground/excited states (red arrow), potential Orbach pathway (green arrow), and the most probable relaxation pathway (blue arrow). Associated numbers indicate mean absolute values of corresponding magnetic transition moment matrix elements.

However, in model **1c**, despite its small size and absence of non-planar equatorial ligands, the Ucal value does not significantly increase in the presence of the Cl^- ligand. Therefore, the axial ligand must be small and strong to achieve a remarkably high barrier height. To investigate the impact of axial ligand bulkiness on U_{cal}, two complexes were optimized with ligands OPh_^{t}Bu$_2$ (model **1f**) and OPh_^{t}Bu$_3$ (model **1 g**); These ligands are similar, differing only in the presence of two tertiary butyl groups in model **1f** and three in model **1 g** As a result, in model **1f**, one side of the equatorial ligands is planar while the other side is non-planar. In contrast, both sides of the equatorial ligands are non-planar in model **1 g** due to much bulkier ligands (Fig 5(a, b)). Consequently, model **1 g** exhibits lower U_{cal} compared to model **1f**. Table 1 highlights the significance of planarity. It demonstrates that as the non-planarity in a molecule increases, there is a corresponding decrease in the barrier height.

To explore the impact of the secondary coordination sphere atoms that are not directly coordinated to the metal in the axial direction, we have examined models **1h, 1i, 1j**, and **1k**, where the Si atom was substituted with C. Surprisingly, this substitution yielded no significant alteration in the U_{cal} value, suggesting that the secondary coordination sphere atom has minimal influence on the barrier height. Further ligands similar to the acetate were also examined, such as acac model (**1a**) and nitrate model (**1b**); here, as well, non-planarity was observed, resulting in diminished SIM characteristics (Fig S9 (c-d). To understand the impact of LoProp charge on U_{cal}, our findings indicate that axial ligands with the same donor atom but a more negative LoProp charge exhibit higher barrier heights. This observation is evident in models **1a, 1b, 1e, 1f, 1 g, 1h, 1i, 1j, 1k, 1l**, while those with a less negative charge tend to have higher barrier heights for equatorial donor atoms shown in Fig S11 (Supporting information).

In summary, an axially asymmetric lanthanide mononuclear complex [DyL^{N6}(Ph_3SiO)(CH_3COO)](PF_6) (**1**) based on Schiff base cyclic ligand (L^{N6}) with the axially asymmetric ligands was synthesized. The complex shows poorer performance compared with the previously reported [DyL^{N6}($Ph_3SiO)_2$](PF_6) with axially symmetric ligands [39]. Through ab initio calculations, it is found that the poor performance of complex **1** is ascribed to the ground state $m_J = \pm 15/2$ mixed with the $m_J = \pm 7/2$ state, which has a small but sufficient transverse anisotropy to trigger quantum tunnelling of magnetization. Moreover, the impact of axial ligands on magnetic properties of complex **1** was investigated. Ligands like F^- and OH^- improve the barrier height, enhancing the SMM performance. Furthermore, the significance of planarity was also explored, revealing that an increase in non-planarity in a molecule corresponds to decreased barrier height. These findings provide valuable insights into enhancing D_{6h} SIM performance.

CRediT authorship contribution statement

Xiang Zhong: Writing – original draft, Investigation. **Rajanikanta Rana:** Writing – original draft, Investigation. **Tong-Kai Luo:** Investigation, Formal analysis. **Yan- Fang Wu:** Investigation, Formal analysis. **Yan Peng:** Writing – review & editing, Supervision, Project administration, Methodology, Funding acquisition. **Sui-Jun Liu:** Writing –

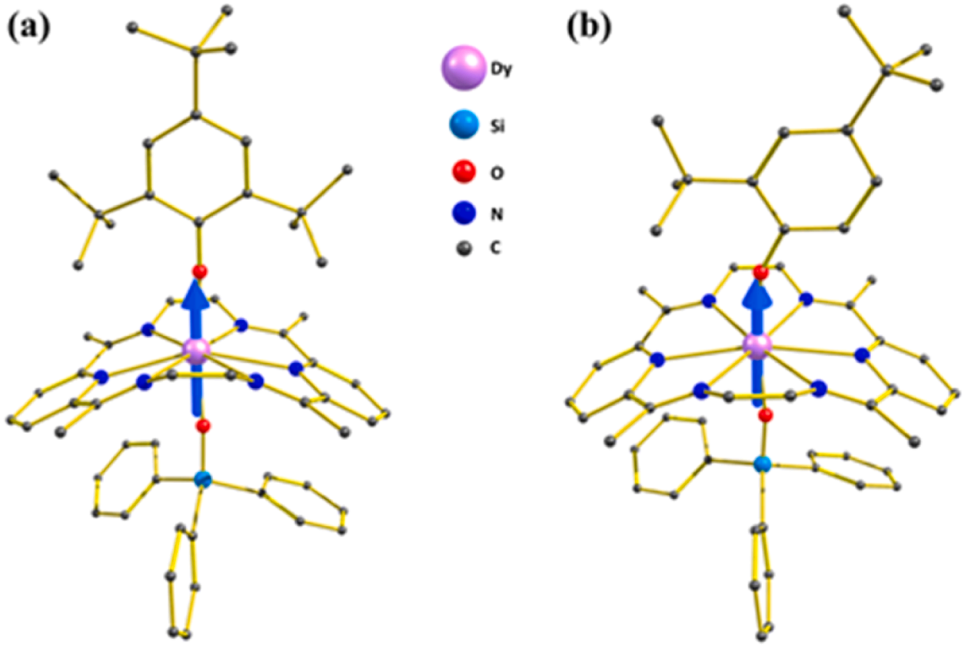

Fig. 5. (a, b) Orientation of the magnetic anisotropy axis (g_{zz}) of **1 g** and **1f**. Hydrogen atoms and solvent molecules are omitted for clarity.

Table 1
Ligands were chosen for this study, along with computed Barrier height (Ucal), Axial crystal field parameters (B_2^0), ground state KD g-tensor, equatorial angle deviation from 180° (φ).

model	Ligand	U_{cal} (cm^{-1})	B_2^0	g_{zz}	φ
1	Crystal	392	10.5	19.967	28.8
1_opt	optimized	402	10.1	19.975	21.7
1a	acac	390	12.7	19.962	26.3
1b	nitrate	373	9.9	19.982	18.6
1c	Cl	365	10.9	19.991	8.9
1d	F	1207	17.5	19.992	7.1
1e	OH	1256	18.8	19.996	6.8
1f	OPh_^{t}Bu$_2$	876	15.9	19.987	14.9
1 g	OPh_^{t}Bu$_3$	795	14.2	19.990	26.6
1h	OSi^{t}Bu	966	18.2	19.991	15.2
1i	O^{t}Bu	984	18.6	19.989	16.1
1j	$OCPh_3$	930	17.9	19.992	12.1
1k	$OSiPh_3$	957	17.3	19.993	15.1
1l	H_2O	346	9.1	19.989	11.9

review & editing, Supervision, Project administration, Funding acquisition. **Gopalan Rajaraman:** Writing – review & editing, Funding acquisition. **He-Rui Wen:** Supervision, Resources, Project administration.

Declaration of competing interest

The authors declare that they have no known competing financial interests or personal relationships that could have appeared to influence the work reported in this paper.

Acknowledgements

This work was supported from the National Natural Science Foundation of China (22261022 and 22261021), the Natural Science Foundation of Jiangxi Province (20224BAB203002 and 20242BAB23018), the Jiangxi Provincial Key Laboratory of Functional Crystalline Materials Chemistry (2024SSY05161), the Youth Jinggang Scholars Program in Jiangxi Province (QNJG2019053), the Double Thousand Talents Program in Jiangxi Province (jxsq2019201068 and jxsq2020101087) and the Doctor's Starting Research Foundation of Jiangxi University of Science and Technology (205200100536). GR thank DST and SERB (CRG/2022/001697 and SB/SJF/2019–20/12) for funding. R.R. thanks PMRF for the fellowship and IITB for the computing facility.

Supplementary materials

Supplementary material associated with this article can be found, in the online version, at doi:10.1016/j.molstruc.2025.142270.

Appendix A. Supplementary data

CCDC 2283969 (**1**) contains the supplementary crystallographic data of this paper. These data can be obtained free of charge via www.ccdc.cam.ac.uk/data_request/cif, or by emailing data_request@ccdc.cam.ac.uk, or by contacting The Cambridge Crystallographic Data Centre, 12 Union Road, Cambridge CB2 1EZ, UK; fax: +44 1223 336033.

Data availability

Data will be made available on request.

References

[1] F.D. Natterer, K. Yang, W. Paul, P. Willke, T. Choi, T. Greber, A.J. Heinrich, C. P. Lutz, Nature 543 (2017) 226–228.
[2] R. Sessoli, Nature 543 (2017) 189–190.
[3] M. Atzori, R. Sessoli, J. Am. Chem. Soc. 141 (2019) 11339. –1135.
[4] F.Luis A.Gaita-Ariño, S. Hill, E. Coronado, Nat. Chem. 11 (2019) 301–309.
[5] A. Candini, S. Klyatskaya, M. Ruben, W. Wernsdorfer, M. Affronte, Nano Lett 11 (2011) 2634–2639.
[6] S. Sanvito, Chem. Soc. Rev. 40 (2011) 3336–3355.
[7] E. Cremades, S. Gomez-Coca, D. Aravena, S. Alvarez, E. Ruiz, J. Am. Chem. Soc. 134 (2012) 10532–10542.
[8] R. Sessoli, Angew. Chem., Int. Ed. 51 (2012) 43–45.
[9] N. Ishikawa, M. Sugita, T. Ishikawa, S. Koshihara, Y. Kaizu, J. Am. Chem. Soc. 125 (2003) 8694–8695.
[10] N. Ishikawa, M. Sugita, W. Wernsdorfer, Angew. Chem., Int. Ed. 44 (2005) 2931–2935.
[11] R. Sessoli, A.K. Powell, Coord. Chem. Rev. 253 (2009) 2328–2341.
[12] D.N. Woodruff, R.E. Winpenny, R.A. Layfield, Chem. Rev. 113 (2013) 5110–5148.
[13] K.S. Pedersen, J. Bendix, R. Clérac, Chem. Commun. 50 (2014) 4396–4415.
[14] K. Liu, X. Zhang, X. Meng, W. Shi, P. Cheng, A.K. Powell, Chem. Soc. Rev. 45 (2016) 2423–2439.

[15] F.S. Guo, B.M. Day, Y.C. Chen, A.Mansikkamäki M.L.Tong, R.A. Layfield, Science 362 (2018) 1400–1403.
[16] C.A.P. Goodwin, F. Ortu, D. Reta, N.F. Chilton, D.P. Mills, Nature 548 (2017) 439–442.
[17] K.L.M. Harriman, J.L. Brosmer, L. Ungur, P.L. Diaconescu, M. Murugesu, J. Am. Chem. Soc. 139 (2017) 1420–1423.
[18] Z.H. Zhu, X. Ying, C. Zhao, Y.Q. Zhang, J.K. Tang, Inorg. Chem. Front. 9 (2022) 6061–6066.
[19] K. Katoh, S. Yamashita, N. Yasuda, Y. Kitagawa, B.K. Breedlove, Y. Nakazawa, M. Yamashita, Angew. Chem., Int. Ed. 57 (2018) 9262–9267.
[20] J.F. Wu, J. Jung, P. Zhang, H.X. Zhang, J.K. Tang, B. LeGuennic, Chem. Sci. 7 (2016) 3632–3639.
[21] S.D. Jiang, B.W. Wang, G. Su, Z.M. Wang, S. Gao, Angew. Chem., Int. Ed. 49 (2010) 7448–7451.
[22] X.L. Ding, Y.Q. Zhai, T. Han, W.P. Chen, Y.S. Ding, Y.Z. Zheng, Chem. Eur. J. 27 (2021) 2623–2627.
[23] M.J. Giansiracusa, A.B. Susan, K.K. Andreas, F.S. George, D.C. Whitehead, F. Tuna, R.E. Winpenny, F.C. Nicholas, Dalton Trans 48 (2019) 10795–10798.
[24] J. Long, A.N. Selikhov, E. Mamontova, K.A. Lyssenko, Y. Guari, J. Larionova, A. Trifonov, Dalton Trans 49 (2020) 4039–4043.
[25] Y.S. Ding, N.F. Chilton, R.E.P. Winpenny, Y.Z. Zheng, Angew. Chem., Int. Ed. 55 (2016) 16071–16074.
[26] J. Liu, Y.C. Chen, J.L. Liu, V. Vieru, L. Ungur, J.H. Jia, L.F. Chibotaru, Y.H. Lan, W. Wernsdorfer, S. Gao, X.M. Chen, M.L. Tong, J. Am. Chem. Soc. 138 (2016) 5441–5450.
[27] Y.C. Chen, J.L. Liu, L. Ungur, J. Liu, Q.W. Li, L.F. Wang, Z.P. Ni, L.F. Chibotaru, X. M. Chen, M.L. Tong, J. Am. Chem. Soc. 138 (2016) 2829–2837.
[28] Z.J. Jiang, L. Sun, Q. Yang, B. Yin, H.S. Ke, J. Han, Q. Wei, G. Xie, S.P. Chen, J. Mater. Chem. C 6 (2018) 4273–4280.
[29] B. Zhang, X.F. Guo, P.F. Tan, W. Lv, X.Y. Bai, Y. Zhou, A.H. Yuan, L. Chen, D. Liu, H.H. Cui, R.S. Wang, X.T. Chen, Inorg. Chem. 61 (2022) 19726–19734.
[30] Y.S. Ding, K.X. Yu, D. Reta, F. Ortu, R.E.P. Winpenny, Y.Z. Zheng, N.F. Chilton, Nat. Commun. 9 (2018) 3134.
[31] K.X. Yu, J.G.C. Kragskow, Y.S. Ding, Y.Q. Zhai, D. Reta, N.F. Chilton, Y.Z. Zheng, Chem 6 (2020) 1777–1793.
[32] X.L. Ding, Q.C. Luo, Y.Q. Zhai, X.F. Zhang, Y. Lv, X.L. Zhang, C. Ke, C. Wu, Y. Z. Zheng, Chin. J. Chem. 40 (2022) 563–570.
[33] Y.S. Ding, T. Han, Y.Q. Zhai, D. Reta, N.F. Chilton, R.E.P. Winpenny, Y.Z. Zheng, Chem. Eur. J. 26 (2020) 5893–5902.
[34] Z.H. Zhu, C. Zhao, T.T. Feng, X.D. Liu, X. Ying, X.L. Li, Y.Q. Zhang, J.K. Tang, J. Am. Chem. Soc. 143 (2021) 10077–10082.
[35] Z.H. Zhu, C. Zhao, Q. Zhou, S.T. Liu, X.L. Li, A. Mansikkamäki, J.K. Tang, CCS Chem 4 (2022) 3762–3771.
[36] Z.H. Li, Y.Q. Zhai, W.P. Chen, Y.S. Ding, Y.Z. Zheng, Chem. Eur. J. 25 (2019) 16219–16224.
[37] S.T. Liu, Y. Gil, C. Zhao, J.J. Wu, Z.H. Zhu, X.L. Li, D. Aravena, J.K. Tang, Inorg. Chem. Front. 9 (2022) 4982–4989.
[38] X.J. Zhou, H.L. Qin, Z.P. Zeng, S.C. Luo, T. Yang, P.P. Cen, X.Y. Liu, Dalton Trans 53 (2024) 16219–16228.
[39] Z.H. Zhu, G.Q. Jin, J.J. Wu, X. Ying, C. Zhao, J.L. Zhang, J.K. Tang, Inorg. Chem. Front. 9 (2022) 5048–5054.
[40] Y. Ma, Y.Q. Zhai, Q.C. Luo, Y.S. Ding, Y.Z. Zheng, Angew. Chem. Int. Ed. 61 (2022) e202206022.
[41] X. Zhong, D.Y. Li, C. Cao, T.K. Luo, Z.B. Hu, Y. Peng, S.J. Liu, Y.Z. Zheng, H.R. Wen, Inorg. Chem. 63 (2024) 21909–21918.
[42] W.J. Xu, Q.C. Luo, Z.H. Li, Y.Q. Zhai, Y.Z. Zheng, Adv. Sci. 11 (2024) 2308548.
[43] Y.S. Ding, W.J.A. Blackmore, Y.Q. Zhai, M.J. Giansiracusa, D. Reta, R.E.P. Winpenny I.V.Yrezabal, N.F. Chilton, Y.Z. Zheng, Inorg. Chem. 61 (2022) 227–235.
[44] Z.H. Zhu, Y.Q. Zhang, X.L. Li, M. Guo, J.J. Lu, S.T. Liu, R.A. Layfield, J.K. Tang, CCS Chem 3 (2021) 388–398.
[45] C.A. Gould, K.R. McClain, D. Reta, J.G.C. Kragskow, D.A. Marchiori, E. Lachman, E. S. Choi, J.G. Analytis, R.D. Britt, N.F. Chilton, B.G. Harvey, J.R. Long, Science 375 (2022) 198–202.
[46] X.W. Cai, Z.J. Cheng, Y.Y. Wu, R. Jing, S.Q. Tian, L. Chen, Z.Y. Li, Y.Q. Zhang, H. H. Cui, A.H. Yuan, Inorg. Chem. 61 (2022) 3664–3673.
[47] A.B. Canaj, S. Dey, E.R. Martí, C. Wilson, G. Rajaraman, M. Murrie, Angew. Chem., Int. Ed. 58 (2019) 14146–14151.